Limitations of the deconvolutional imaging condition for two-way propagators

Ning Tu, Tristan van Leeuwen and Felix J. Herrmann, Earth and Ocean Sciences, University of British Columbia

SUMMARY

The deconvolutional imaging condition has gained wide attention in recent years, as it is often used to image surface-related multiples. However, we noticed on close inspection that this condition was derived from one-way propagation principles. Now that two-way wave-equation based simulations have become more affordable , we revisit the deconvolutional imaging condition and reveal its limitations for two-way propagators. First, it can distort the image due to receiver-side propagation effects. Second, when used to image surface-related multiples, it is not capable of removing all interfering phantom reflectors.

INTRODUCTION

Surface-related multiples in marine acquisition can be strong enough to interfere with the primary reflections. If not handled correctly, they can result in phantom reflectors that hinders correct interpretation. On the other hand, if correctly used, they can provide additional information on the subsurface. Based on the SRME formulation (Verschuur et al., 1992), multiples can be identified as the seismic response given the total down-going wavefield at the surface as the source wavefield (Berkhout, 1993). However, even with the source wavefield correctly identified, imaging multiples still remains a challenge as the cross-correlation imaging condition fails to yield an artifacts-free seismic image due to non-causal cross-correlations (Muijs et al., 2007; Liu et al., 2011). To address the issue, some researchers proposed to use the deconvolutional imaging condition (or the smoothing imaging condition derived from it) (Claerbout, 1971; Guitton et al., 2007; Muijs et al., 2007; Whitmore et al., 2010; Lu et al., 2011), while others suggested that an inversion approach (e.g., least-squares migration) should be used (Verschuur, 2011; Tu and Herrmann, 2012).

The deconvolutional imaging condition was derived from one-way propagation principles (Claerbout, 1971). Now that the two-way wave-equation based simulations have become more affordable, we scrutinize the applicability of the deconvolutional imaging condition for two-way propagators. Our contribution is organized as follows. First, we do a theoretical analysis of the deconvolutional imaging condition in the context of one-way and two-way wave propagations. As it is extensively used to image surface-related multiples, we continue to examine its efficacy for imaging surface-related multiples, and compare it with our linearized inversion approach, namely the sparsity promoting migration with surface-related multiples (Herrmann and Li, 2012; Tu and Herrmann, 2012).

A THEORETICAL ANALYSIS

For simplicity, we use the detail-hiding matrix notation to describe the one-way wave propagation (Berkhout and Wapenaar, 1993). Tensor $\mathbf{U}^+$ is the down-going wavefield, obtained by downward propagating the down-going source wavefield $\mathbf{S}^+$, and $\mathbf{V}^-$ is the up-going wavefield, obtained by downward propagating the upgoing receiver wavefield $\mathbf{D}^-$. In frequency domain modelling, both $\mathbf{U}^+$ and $\mathbf{V}^-$ are representations of the physical position (x,z), the source indexed by i, and the frequency indexed by j. Denoting the monochromatic downward continuation operator as $\mathbf{W}_j^+$, and the upward continuation operator as $\mathbf{W}_j^-$, and the reflectivity operator as $\mathbf{R}_{(i,j)}$, we have $\mathbf{U}_{(i,j)}^+ = \mathbf{W}_j^+ \mathbf{S}_{(i,j)}^+$ and the receiver wavefield $\mathbf{D}_{(i,j)}^- = \mathbf{W}_j^- \mathbf{R}_{(i,j)} \mathbf{W}_j^+ \mathbf{S}_{(i,j)}^+$. Note that with fixed indices i, j, all wavefields here are vectors. In cases where the exact inverse of the upward continuation operator $\mathbf{W}_j^-$ can be derived so that $\mathbf{V}_{(i,j)}^- = (\mathbf{W}_j^-)^{-1} \mathbf{D}_{(i,j)}^-$, the deconvolutional imaging condition can be put as (Claerbout, 1971)

$$\begin{aligned} \tilde{\mathbf{R}} &= \sum_{i,j} \mathbf{V}_{(i,j)}^- / \mathbf{U}_{(i,j)}^+ \\ &= \sum_{i,j} \frac{(\mathbf{W}_j^-)^{-1} \mathbf{W}_j^- \mathbf{R}_{(i,j)} \mathbf{W}_j^+ \mathbf{S}_{(i,j)}^+}{\mathbf{W}_j^+ \mathbf{S}_{(i,j)}^+} \\ &= \sum_{i,j} \mathrm{diag}(\mathbf{R}_{(i,j)}), \end{aligned} \tag{1}$$

where $\tilde{\mathbf{R}}$ is the reconstructed image, the division is performed in a element-wise manner, $\mathbf{R}$ is a diagonal operator with the reflectivity coefficients on the diagonal entries (Verschuur and Berkhout, 2009), and notation "diag" means to obtain the diagonal entries of a matrix. In this case, the image is a summation of the reflectivities for all sources and frequencies, and is therefore accurate. However, as pointed out by Gray (1997), $(\mathbf{W}_j^-)^*$ (star means the adjoint) is often used in practice due to stability issues when inverting $\mathbf{W}_j^-$. In this case, the image can be distorted due to receiver side propagation effects embodied in $(\mathbf{W}_j^-)^* \mathbf{W}_j^-$.

Now we turn to two-way wave-equation migrations. A fundamental difference from its one-way counterpart is that an image is *not* formed from the reflectivity, but rather from the perturbation in medium parameters $\delta\mathbf{m}$ over a background medium $\mathbf{m}_0$. Instead of having the up-going wavefield $\mathbf{U}^+$ and down-going wavefield $\mathbf{V}^-$ by downward continuation, we now have the temporally forward propagated source wavefield $\mathbf{U}$ and backward propagated receiver wavefield $\mathbf{V}$. Denoting the time-harmonic Helmholtz operator as $\mathbf{H}_j = \mathbf{H}[\mathbf{m}_0, \omega_j]$, we can write $\mathbf{U}_{(i,j)} = \omega_j \mathbf{H}_j^{-1} \mathbf{S}_{(i,j)}$. By writing $\mathbf{W}_j \doteq \omega_j \mathbf{H}_j^{-1}$ here, we have $\mathbf{U}_{(i,j)} = \mathbf{W}_j \mathbf{S}_{(i,j)}$, and the linearized receiver wavefield

$$\mathbf{D}_{(i,j)} = \mathbf{W}_j \mathrm{diag}(\delta\mathbf{m}) \mathbf{W}_j \mathbf{S}_{(i,j)}.$$

Here we overload the notation "diag" to mean inserting a vector into the diagonal entries of a matrix. Now we clearly see the analogue between the one-way and two-way propagators. By time-reversely propagating the receiver wavefield, we have

$$\mathbf{V}_{(i,j)} = \omega_j (\mathbf{H}_j^{-1})^* \mathbf{D}_{(i,j)} = \mathbf{W}_j^* \mathbf{D}_{(i,j)}.$$

Note that the adjoint operation in the frequency domain corresponds to a reversal in time. Since the adjoint of $\mathbf{W}_j$ is used,

the propagation effects on the receiver side can distort the image if the deconvolutional imaging condition is applied.

On the other hand, the cross-correlation imaging condition for two-way propagators remains the adjoint of the linearized forward modelling. As the deconvolutional imaging condition is often regarded as an "inversion" scheme (see Guitton et al., 2007, equation (3)), we also compare the approach with our linearized inversion approach, where we invert the linearized Born scattering operator by promoting Curvelet sparsity in the model space (Herrmann and Li, 2012). With the notations written above, the monochromatic linearized Born scattering operator $\nabla\mathbf{F}_j$ is expressed as:

$$\mathbf{W}_j \text{diag}(\delta\mathbf{m})\mathbf{W}_j\mathbf{S}_j \doteq \nabla\mathbf{F}_j\delta\mathbf{m},$$

and is a function of the monochromatic source wavefield $\mathbf{S}_j$ and the background model $\mathbf{m}_0$.

Since the deconvolutional imaging condition is plagued by zeros in the denominator (see equation (1)), in our examples we use either the damped version (Claerbout, 1971):

$$\tilde{\mathbf{R}} = \sum_{i,j} \frac{\mathbf{V}_{(i,j)}\mathbf{U}^*_{(i,j)}}{\|\mathbf{U}_{(i,j)}\|_2^2 + \varepsilon}, \tag{2}$$

with $\varepsilon = \lambda * \text{mean}(\|\mathbf{U}_{(i,j)}\|_2^2)$, or alternatively the smoothing imaging condition (Guitton et al., 2007):

$$\tilde{\mathbf{R}} = \sum_{i,j} \frac{\mathbf{V}_{(i,j)}\mathbf{U}^*_{(i,j)}}{< \|\mathbf{U}_{(i,j)}\|_2^2 >_{(x,z)}}, \tag{3}$$

where the symbol $<>_{x,z}$ means smoothing vertically and horizontally over a window.

Stylized example

We design the following experiment to verify our theoretical analysis. The background model we use is shown in Figure (1(a)). The left and the right halves are symmetric. There are 3000m/s velocity anomalies (boundaries are smoothed) over a background velocity of 1500m/s. The model perturbation is shown in Figure (1(b)). The model is 594m deep and 1194m wide with six meter grid distance. There are 50 sources put on the left side and 50 receivers symmetrically put on the right side at six meters in depth with 12-meter lateral spacing. By designing such a model and acquisition geometry, the waves to image the left half of the perturbation are more affected by the source-side propagation effects, while the right half is more affected by the receiver-side effects. We generate data by applying the linearized Born scattering operator $\nabla\mathbf{F}$ to the true model perturbation $\delta\mathbf{m}$. A Ricker wavelet of 20Hz peak frequency is used.

We compare three scenarios here. In the first scenario, we obtain a baseline RTM image. In the second scenario, we use two-way propagators, but use the damped deconvolutional imaging condition (equation 2), with the damping parameter $\lambda = 0.05$, and the smooth imaging condition (equation 3), with a 100-meter smoothing window. In the third scenario, we run our sparsity promoting migration with all the data for 100 iterations. The results are shown in Figure (1(c)) to (1(f)).

Comparing the images, we can see that the deconvolutional imaging condition, as well as its smoothing variant, lead to wrong positions of the model perturbation on the right half of the model (indicated by arrows). Combining this observation with our theoretical analysis, we conclude that for two-way propagators, the deconvolutional imaging condition can distort the image due to receiver side propagation effects. On the other hand, both RTM and the linearized inversion give us correct images.

IMAGING SURFACE-RELATED MULTIPLES

Most applications of the deconvolutional imaging condition that we are interested in are to image surface-related multiples, where it is used somewhat as an "invesion" approach. Now we have shown that it is not really an inversion approach, we are going to investigate its plausibility in imaging multiples by comparing it with the linearized inversion approach.

However, linearized inversion for a model of realistic dimensions is usually considered to be computationally unaffordable as it requires repeated evaluations of the Born scattering operator and its adjoint, while each evaluation itself is already expensive by having to solve four PDEs for each monochromatic source experiment. In the case of imaging multiples, the computational cost is significantly increased by performing multi-dimensional convolution for multiple prediction. However, we have shown that the computational cost can be greatly reduced by (Tu and Herrmann, 2012): i) identifying the total downgoing wavefield at the surface (i.e., $\mathbf{D}$ with our notation) as the generalized areal source, and letting the wave-equation solver to carry out the multi-dimensional convolution implicitly, and ii) reducing per-iteration simulation cost by using simultaneous sources and randomized subsets of frequencies. By introducing *rerandomization* (Tu and Herrmann, 2012), the computational cost can be further reduced without compromising the image quality. Here we use these techniques to achieve a fast inversion.

Example

We use a more realistic model cropped from the sedimentary part of the Sigsbee 2B model (courtesy of the SMAART JV). The background model is shown in Figure (2(a)), and the true model perturbation is shown in Figure (2(b)). The model is 3.8km deep and 5.9km wide, with 7.62m grid spacing. There are 261 co-located sources and receivers at a depth of 7.62m with 22.86m lateral spacing. We generate the surface-related multiples by applying the linearized Born scattering operator with generalized source $\nabla\mathbf{F}[\mathbf{m}_0, \mathbf{D}]$ to the true model perturbation $\delta\mathbf{m}$. We model the total data $\mathbf{D}$ using a time-domain finite difference code with a free-surface boundary condition.

We do the same comparisons as we did for the stylized example. We skip the smoothing imaging condition as it well approximates the deconvolutional imaging condition (e.g., compare Figure (1(d)) and (1(e))). The damping parameter λ for the deconvolutional imaging is tweaked to be 0.4 (a smaller λ yields to instability in division). In our sparsity promoting migration, we use 15 frequencies, 8 simultaneous sources, and run 338 iterations. This leads to a simulation cost roughly the *same* as a single RTM of all the data. The results are shown in

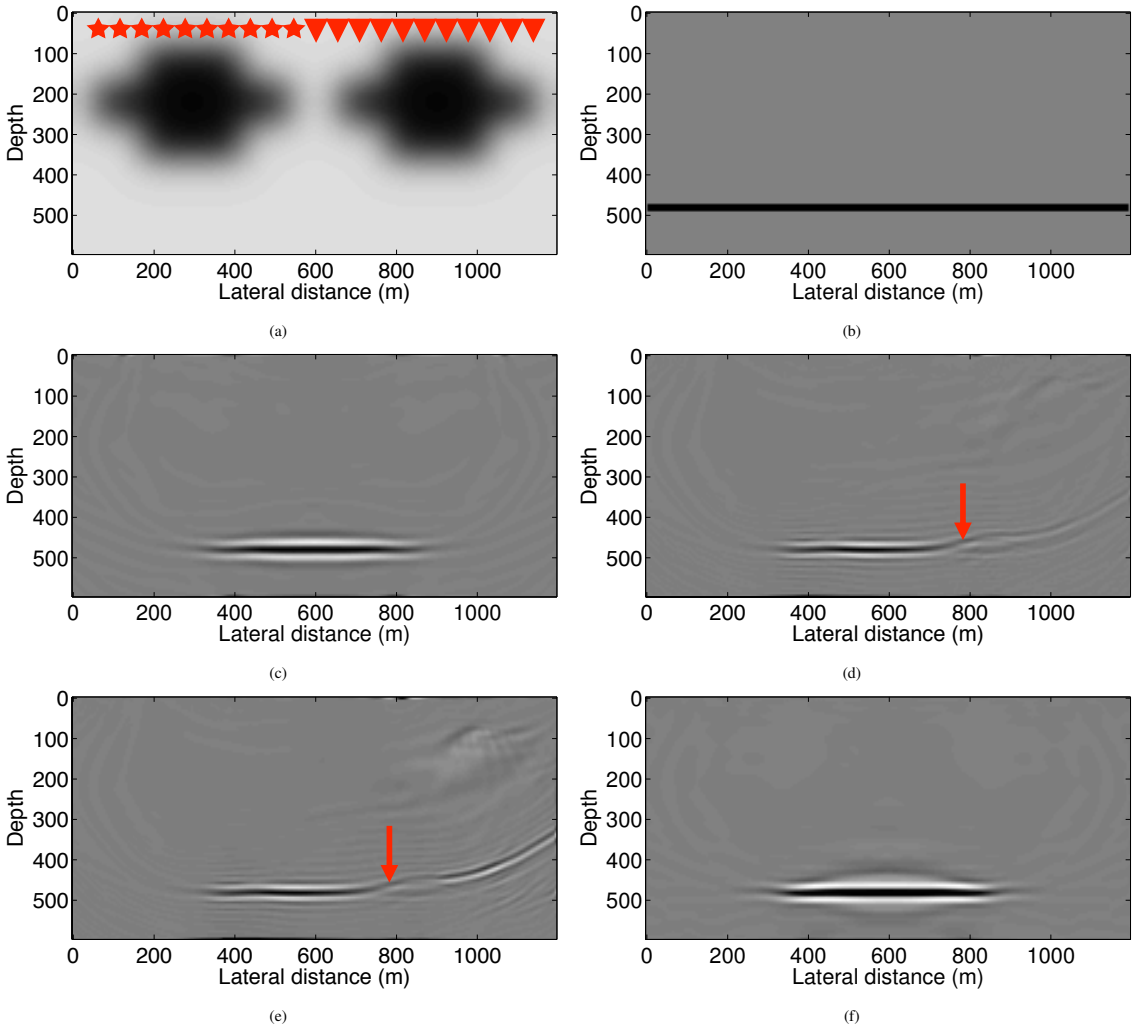

Figure 1: The model and the imaging results of the stylized example. The arrow in **(d)** or **(e)** indicates the image distortion. **(a)**. The background model, stars indicate source positions and triangles indicate receivers. **(b)**. True model perturbation. **(c)**. The RTM image. **(d)**. Image by the deconvolutional imaging condition. **(e)**. Image by the smoothing imaging condition. **(f)**. Image by sparsity promoting migration.

Figure (2(c)) to (2(e)).

Many authors have concluded that for multiples, the cross-correlation imaging condition (e.g., RTM) introduces artifacts caused by non-causal cross-correlations (a replicate of the ocean bottom reflection is indicated by the arrow in Figure (2(c)), see Muijs et al., 2007; Liu et al., 2011, for details). Now from Figure (2(d)), we can see that the deconvolutional imaging condition is neither the right choice (the ocean bottom replicate is again indicated by an arrow). The same artifact is also observed by Muijs et al. (2007) (Figure 11b) using one-way propagators. On the other hand, we do get an virtually artifact-free image with our method.

CONCLUSION

We analyzed the limitations of the deconvolutional imaging condition for two-way propagators. We showed that it can distort the image due to receiver-side propagation effects. When used to image the surface-related multiples, it fails to yield an image free of coherent artifacts as it is not really an inversion approach. In light of this, a true inversion scheme is necessary to image the surface-related multiples, and this can be done efficiently using our fast sparsity promoting migration approach with rerandomization.

ACKNOWLEDGEMENT

This work was in part financially supported by the Natural Sciences and Engineering Research Council of Canada Discovery Grant (22R81254) and the Collaborative Research and Development Grant DNOISE II (375142-08). This research was carried out as part of the SINBAD II project with support from the following organizations: BG Group, BGP, BP, Chevron, ConocoPhillips, Petrobras, PGS, Total SA, and WesternGeco. The authors would like to thank the SMAART JV for sharing the Sigsbee 2B model. Ning Tu also receives a scholarship from the China Scholarship Council.

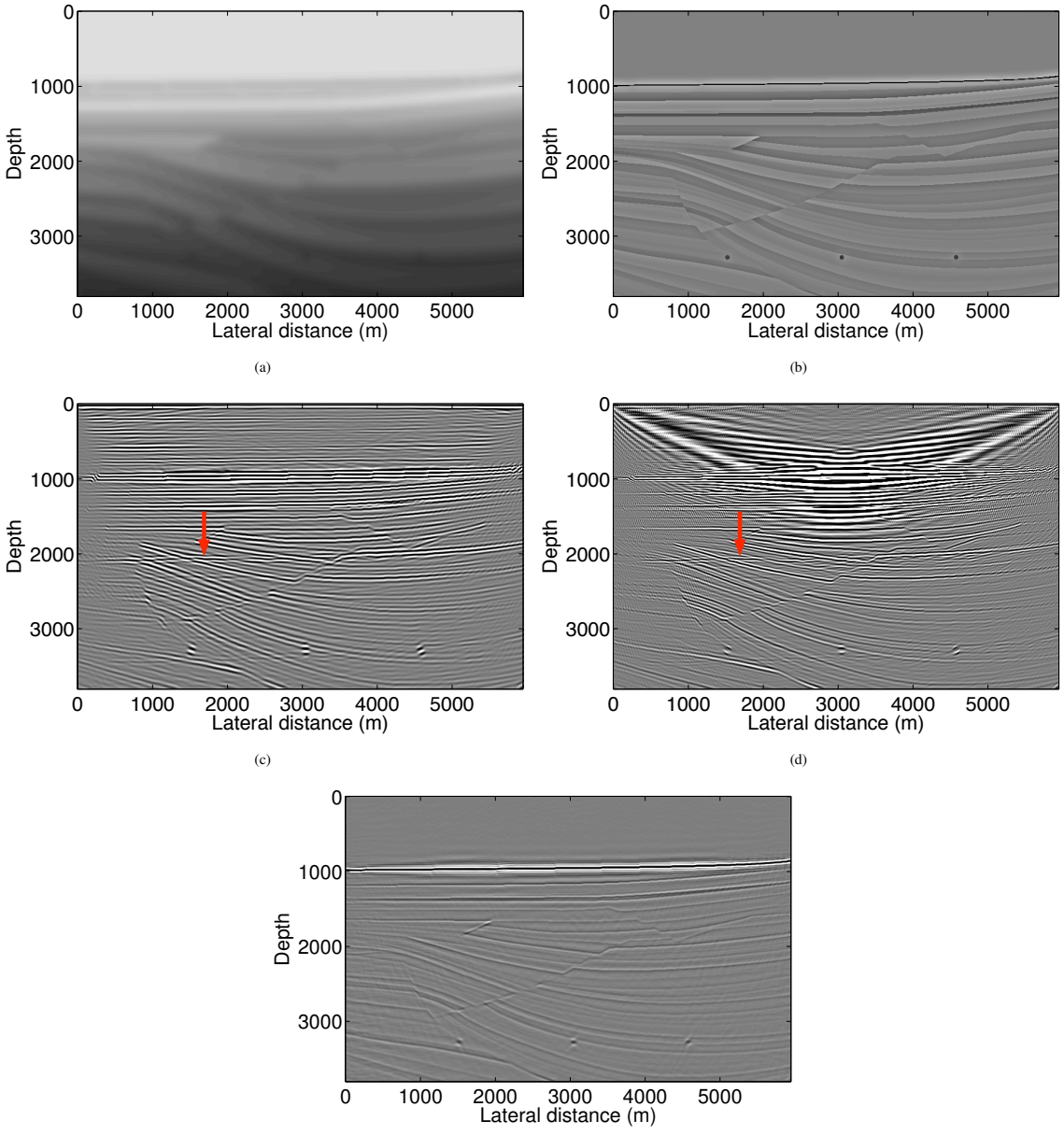

Figure 2: The model and the images of surface-related multiples. The arrow in **(c)** or **(d)** indicates a replicate of the ocean bottom reflection. **(a)**. The background model. **(b)**. True model perturbation. **(c)**. The RTM image. **(d)**. Image by the deconvolutional imaging condition. **(e)**. Image by our fast sparsity promoting migration, where the simulation cost is roughly the same as in **(c)** or **(d)**.

REFERENCES

Berkhout, A. J., 1993, Migration of multiple reflections: SEG Technical Program Expanded Abstracts, 1022–1025.

Berkhout, A. J., and C. P. A. Wapenaar, 1993, A unified approach to acoustical reflection imaging. ii: The inverse problem: The Journal of the Acoustical Society of America, **93**, 2017–2023.

Claerbout, J. F., 1971, Towards a unified theory of reflector mapping: Geophysics, **36**, 467–481.

Gray, S. H., 1997, True-amplitude seismic migration: A comparison of three approaches: Geophysics, **62**, 929–936.

Guitton, A., A. Valenciano, D. Bevc, and J. Claerbout, 2007, Smoothing imaging condition for shot-profile migration: Geophysics, **72**, S149–S154.

Herrmann, F. J., and X. Li, 2012, Efficient least-squares imaging with sparsity promotion and compressive sensing: Geophysical Prospecting, **60**, 696–712.

Liu, Y., X. Chang, D. Jin, R. He, H. Sun, and Y. Zheng, 2011, Reverse time migration of multiples for subsalt imaging: Geophysics, **76**, WB209–WB216.

Lu, S., N. D. Whitmore, and A. A. Valenciano, 2011, Imaging of primaries and multiples with 3d seam synthetic: SEG Technical Program Expanded Abstracts, 3217–3221.

Muijs, R., J. O. A. Robertsson, and K. Holliger, 2007, Prestack depth migration of primary and surface-related multiple reflections: Part i—imaging: Geophysics, **72**, S59–S69.

Tu, N., and F. J. Herrmann, 2012, Imaging with multiples accelerated by message passing: Presented at the SEG Technical Program Expanded Abstracts, SEG.

Verschuur, D. J., 2011, Seismic migration of blended shot records with surface-related multiple scattering: Geophysics, **76**, A7–A13.

Verschuur, D. J., and A. J. Berkhout, 2009, Target-oriented, least-squares imaging of blended data: SEG Technical Program Expanded Abstracts, 2889–2893.

Verschuur, D. J., A. J. Berkhout, and C. P. A. Wapenaar, 1992, Adaptive surface-related multiple elimination: Geophysics, **57**, 1166–1177.

Whitmore, N. D., A. A. Valenciano, and W. Sollner, 2010, Imaging of primaries and multiples using a dual-sensor towed streamer: SEG Technical Program Expanded Abstracts, 3187–3192.